Solution Structure, Stability, and Nucleic Acid Binding of the Hyperthermophile Protein Sso10b2[†,‡]

Kalpesh Biyani, Mebrahtu A. Kahsai, Andrew T. Clark, Tracy L. Armstrong, Stephen P. Edmondson,* and John W. Shriver*

Laboratory for Structural Biology, Departments of Chemistry and Biological Sciences, Graduate Program in Biotechnology and Bioengineering, University of Alabama in Huntsville, Huntsville, Alabama 35899

Received July 1, 2005; Revised Manuscript Received September 1, 2005

ABSTRACT: The Sso10b (or Alba) family of proteins is a conserved group of archaeal and eukaryotic proteins which are thought to play a role in both chromatin organization and RNA metabolism. We describe here the solution structure and properties of Sso10b2 from *Sulfolobus solfataricus*. NMR data including residual dipolar couplings and ^{15}N relaxation data demonstrated that the protein adopts a $\beta_1\alpha_1\beta_2\alpha_2\beta_3\beta_4$ topology with an IF-3-like fold. The protein dimerizes in solution at 30 °C via a hydrophobic surface defined by the C-terminal $\alpha_2\beta_3\beta_4$ elements with a structure similar to one of the putative dimers indicated by previous crystal structures. DSC and circular dichroism data demonstrated an unusual two-state structural transition near the growth temperature which led to an increase in β-sheet content without dissociation of the dimer. The cooperativity of the transition exceeded that of a dimer at pH 7, demonstrating the presence of higher order oligomers near the growth temperature at pH 7. Reverse titrations of Sso10b2 with nucleic acid showed that the protein binds single-stranded DNA (K_d of 3×10^{-7} M) with higher affinity than RNA (1.3×10^{-6} M) or double-stranded DNA (1.5×10^{-5} M) in 10 mM KH_2PO_4 (pH 7.0, 20 °C). NMR chemical shift perturbation data indicated that single-stranded DNA and RNA binding occurred across the same dimer interface and encompassed a surface defined by the C-terminal ends of the β_1, β_2, and β_3 strands of each monomer.

The Sso10b family of proteins were originally isolated from the archaeon *Sulfolobus solfataricus* (*1*) and have been shown to be associated with both RNA and DNA in vivo in this hyperthermophile (*2*, *3*). Their exact function is unknown, but close association with Sir2 and specific lysine acetylation indicates a potential role in the regulation of chromatin structure and gene regulation (*3*, *4*). Homologous proteins exist not only in the thermophilic archaea but also in a number of eukaryotes, including *Arabidopsis thaliana* and *Homo sapiens* (see, for example, EMBL-EBI IPR002775) (Figure 1). No homologues have been identified in the eubacteria. More than one homologous gene is often found in a number of species including five in the human genome (*5*−*7*). *S. solfataricus* expresses two distantly related Sso10b proteins, Sso10b and Sso10b2, with molecular weights of 10 973 and 10 239, respectively (*6*, *7*). Electron micrographs showed Sso10b to form highly ordered protein−DNA complexes which were modeled as two strands of protein wrapped around a DNA duplex (*8*). Increased interest in Sso10b resulted from a report which indicated that acetylation of a specific lysine led to a 10-fold reduction in DNA binding affinity (*4*). Sso10b was therefore renamed Alba (acetylation lowers binding affinity), and the family of proteins is now often identified with this name. Recent data indicate that the effect of acetylation is significantly less (*3*), or nil (*2*), and the role of acetylation is now unclear.

A possible role of Sso10b in RNA metabolism was indicated by electron microscopy which showed that DBNP-B (presumed to be Sso10b) was associated with the ribosomes in *Sulfolobus* (*9*, *10*). Following this observation, it was demonstrated that Ssh10b (a homologue from *Sulfolobus shibatae*) was cross-linked by UV irradiation exclusively to RNA in vivo, and that it was associated with ribosomal RNA even in the absence of UV irradiation (*2*). In vitro binding experiments demonstrated that Ssh10b bound to RNA with an affinity equal to, or slightly greater than, duplex DNA ($K_d \sim 0.5$ μM) (*2*). Sequence analysis has indicated that the Alba family of proteins originated as RNA binding proteins, and some are expected to still function in RNA metabolism (*7*). Three of the homologous human proteins in IPR0022775 have been classified as RNase P subunits, including p20 or hPOP7 (O75817) and p25 (Q9BUL9).

Little is known about the solution properties of members of the Alba family. Ssh10b has been shown to be a highly thermostable protein with little change in CD up to 90 °C at pH 7 (*11*). Thermal unfolding could be followed by CD only in the presence of relatively high concentrations of GdnHCl (greater than 2.5 M) (*12*). An initial report indicated that the protein was dimeric by gel filtration (0.35 M KCl, pH 7.0) (*1*). Chemical cross-linking studies however showed that

[†] This work was supported by Grant GM49686 from the National Institutes of Health to J.W.S. and S.P.E.

[‡] Coordinates for Sso10b2 have been deposited at the Protein Data Bank (2A2Y).

* Address for correspondence: John W. Shriver or Stephen P. Edmondson, Department of Chemistry, Materials Science Building, John Wright Drive, University of Alabama in Huntsville, Huntsville, AL 35899. Phone, 256-824-2477; fax, 256-824-6349; e-mail, shriverj@uah.edu.

10.1021/bi051266r CCC: $30.25
Published on Web 10/07/2005

Ssh10b formed higher order oligomers (50 mM KCl, pH 7.6) (*11*), and it was concluded that the protein did not exist predominantly in any one oligomeric form.

Five crystal structures of members of the Alba family of proteins have been determined: Sso10b or Alba (1HOX, 1H0Y) (*13*) and Sso10b2 (1UDV) (*14*) from *S. solfataricus*, Afu10b or Af-Alba (1NFJ) (*15*) from *Archaeoglobus fulgidus*, Mja10b (1NH9) (*16*) from *Methanococcus jannaschii*, and a gene product from *A. thaliana* which has not been characterized beyond deposition of coordinates (1VM0). All of the structures have a $\beta\alpha\beta\alpha\beta\beta$ topology and are similar to the C-terminal domain of *Bacillus stearothermophilus* translation initiation factor IF3 (*17*) and the N-terminal DNA binding domain of DNase I (*18*), including an extended β-hairpin that is important in binding to the minor groove of DNA in the DNase I−DNA complex. Protein packing in the various crystal forms indicated at least three different protein−protein interfaces that may play a role in forming dimer and higher order oligomeric interactions in solution. One form in Sso10b showed a buried surface area of approximately 700 Å^2 that was argued to represent a dimer interface (referred to here as interface I) (*13*). A second crystal form exhibited interactions via a different interface (II) with a buried surface area of approximately 460 Å^2, but the significance of this was not explained. Zhao et al. (*15*) argued that the second interface in the *Archeaoglobus* protein is physiologically important in the formation of a tetramer (i.e., a dimer of dimers) that represents the DNA binding species. Recent NMR data on *S. shibatae* Ssh10b indicated that intermolecular NOEs[1] only occurred across interface I, but a detailed solution structure was not presented. A third dimer interface (III) was indicated in the structure of the Alba-like protein from *A. thaliana* (1VM0) and also in Sso10b2 (*14*).

We present here a characterization of the solution structure and properties of Sso10b2. NMR and ultracentrifugation studies show that the protein exists in solution primarily as a dimer below pH 6, with the dimer interface being interface I. Both thermal unfolding and nucleic acid binding indicate additional protein−protein interactions and the formation of higher order oligomers. Surprisingly, the protein is shown to exist in two conformational states near the growth temperature. Transition between the two states is associated with an unusually large enthalpy change and an increase in β-sheet without a change in quaternary structure. The cooperativity of this transition increases with pH, indicating the presence of higher order oligomers.

MATERIALS AND METHODS

Gene Cloning and Expression. The Sso10b2 gene was amplified by PCR from *S. solfataricus* genomic DNA, cloned into pETBlue-2 (Novagen), and expressed in RosettaBlue-(DE3) (Novagen). Uniformly ^{15}N- and/or ^{13}C-enriched protein for NMR was obtained by supplementing minimal media with $^{15}NH_4Cl$ (Isotec) and/or ^{13}C-glucose (Isotec) and growing the cells in a 2 L Bioflo 3000 bioreactor (New Brunswick Scientific, Edison, NJ). Protein expression was induced with IPTG (1 mM), the temperature was reduced to 27 °C for 8−10 h, cells were harvested by centrifugation, and the pellet was stored at −80 °C.

Protein Purification. Frozen cells were thawed and suspended in 100 mL of ice-cold buffer (10 mM EDTA, 10 mM Tris-HCl, pH 8.0, 0.1% Triton X-100, and 0.5 mM PMSF) and lysed by sonication, DNase I (Sigma) was added (0.5 mg/mL), and the suspension was incubated at 37 °C for 5 min. The suspension was then incubated at 70 °C for 40 min to precipitate *Escherichia coli* proteins and the solution clarified by centrifugation at 300 000*g*. The supernatant was filtered (0.45 μm filter), and recombinant Sso10b2 was purified by cation exchange chromatography on a Hi-trap SP (Pharmacia) column equilibrated with 10 mM KH_2PO_4 (pH 7). Sso10b2 eluted at 0.5 M NaCl with a linear 0−1.0 M NaCl gradient. Protein purity and molecular weight were demonstrated by SDS gel electrophoresis. The identity of the protein was confirmed by sequential NMR assignments (see below). The protein concentration was determined using a calculated (*19*) extinction coefficient of 0.375 mL mg^{-1} cm^{-1}.

Analytical Ultracentrifugation. Sedimentation velocity experiments were performed on a Beckman (Fullerton, CA) XL-A analytical ultracentrifuge using two-channel centerpieces with an An60Ti rotor at 59 000 rpm and 20 °C. Sedimentation was monitored using absorption at 230 nm with protein concentrations of 0.056, 0.14, and 0.23 mg/mL in 0.01 M KH_2PO_4 buffer (pH 7.0) with 0.15 M NaCl. The Ultrascan software obtained from the Reversible Associations in Structural and Molecular Biology web site (http://www.bbri.org/RASMB/rasmb.html) was used to check sample homogeneity with the van Holde−Weischet method and to calculate the sedimentation coefficient and protein mass from finite element fitting of the data to a one-component system.

Differential Scanning Calorimetry. DSC measurements were performed using a MicoCal (Northampton, MA) Extended Range VP-DSC with a cell volume of 0.5 mL. Protein samples were dialyzed against an excess of the appropriate buffer for approximately 12 h, and aliquots of protein and dialysis buffer were degassed with stirring under vacuum using the MicroCal accessory. Protein and buffer solutions were scanned at 1.5 °C/min from 5 to 125 °C under an applied pressure of 25 psi to prevent vaporization and bubble formation. Reversibility of thermal unfolding was demonstrated with repeated scans on the same sample.

DSC data were analyzed using an IGOR Pro (Wavemetrics, Oregon) procedure (IgorDenat, available at http://daffy.uah.edu/thermo) with routines that permitted fitting of baselines, ΔC_P, ΔH, and T_m (or T_o) for multiple transitions. The most appropriate model for Sso10b2 thermal unfolding below pH 6 was one with a structural transition between two dimeric native states, both of which unfold to random coil monomeric subunits:

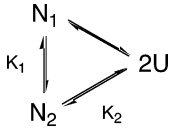

[1] Abbreviations: CSI, chemical shift index; DEPC, diethylpyrocarbonate; DSC, differential scanning calorimetry; NOE, nuclear Overhauser effect; RDC, residual dipolar coupling; R_1, longitudinal relaxation rate ($1/T_1$); R_2, transverse relaxation rate ($1/T_2$); τ_m, overall rotational correlation time; T_1, longitudinal relaxation time; $T_{1\rho}$, rotating frame relaxation time; T_2, transverse relaxation time.

where $K_1 = [N_2]/[N_1]$ and $K_2 = [U]^2/[N_2]$. The total concentration of protein in moles of monomers is given by $c = 2[N_1] + 2[N_2] + [U]$, and the concentration of the unfolded monomer is given by

$$[U] = \frac{-K_1K_2 + \sqrt{K_1K_2}\sqrt{8c(1+K_1) + K_1K_2}}{4(1+K_1)} \quad (1)$$

K_1 is a function of temperature and is related to the free energy of the $N_1 \leftrightarrow N_2$ transition by

$$K_1(T) = \exp[-\Delta G_1^{o}(T)/RT] \quad (2)$$

where

$$\Delta G_1^{o}(T) = \Delta H_1(T)\left(1 - \frac{T}{T_m}\right) + \Delta C_{P1}\left(T - T_m + T\ln\frac{T_m}{T}\right) \quad (3)$$

and

$$\Delta H_1(T) = \Delta H_1(T_m) + \Delta C_{P1}(T - T_m) \quad (4)$$

$$\Delta C_{P1} = \Delta C_P\left(\frac{\Delta H_1}{\Delta H_1 + \Delta H_2}\right) \quad (5)$$

$\Delta H(T_m)$ is the enthalpy change of the reaction at the midpoint temperature, T_m, and ΔC_{P1} is the change in heat capacity calculated by assuming that the total ΔC_P is partitioned between the two reactions (1 and 2) according to their relative enthalpies. The total ΔC_P was fixed to that determined by a global analysis of the chemical denaturation data described below (1961 cal deg^{-1} mol^{-1}). Similar equations apply to $K_2(T)$ describing the $N_2 \leftrightarrow 2U$ reaction with the reference temperature being T_o, the midpoint temperature at 1 M protein concentration. The relative partition function, Q (*20*, *21*), for the total scheme is given by

$$Q = \frac{2N_1 + 2N_2 + U}{2N_1} = 1 + K_1 + \frac{K_1K_2}{2[U]} \quad (6)$$

The fractional populations (α) of the three states is obtained from the partition function in the usual way:

$$\alpha_{N1} = \frac{1}{Q}$$

$$\alpha_{N2} = \frac{K_1}{Q}$$

$$\alpha_U = \frac{K_1K_2}{2[U]Q} \quad (7)$$

Finally, the DSC excess heat capacity is given by the change in the fractional occupation of the states with increasing temperature multiplied by the heat change at that temperature:

$$C_{P,excess} = \frac{d\alpha_U}{dT}\Delta H_2(T) - \frac{d\alpha_{N_1}}{dT}\Delta H_1(T) \quad (8)$$

Chemical Denaturation. Chemical denaturation was monitored by fluorescence anisotropy using tyrosine fluorescence with a Jobin Yvon (Edison, NJ) Fluoromax-3 equipped with automatic polarizers. Fluorescence was detected with 275 nm excitation, 300 nm emission, and 4 nm slit widths. Titrations were performed by adding 50 μL aliquots of a 10 μM protein solution in 8 M guanidine hydrochloride with 0.01 M MOPS (pH 7.0) (the titrant) into a cuvette containing 2.4 mL of a 10 μM protein sample solution in 0.01 M MOPS (pH 7.0) using a Hamilton (Reno, NV) Microlab-500 titrator controlled by computer. Titrations were performed at constant volume by preceding each titrant injection with removal of an equal amount of sample solution. The temperature was controlled with a circulating water bath and was calibrated to within $\pm$0.5 °C in the cuvette. Total data collection time was 2.0 min for each titration point, with a 1.0 min equilibration time. The concentration of guanidine hydrochloride (Mallinckrodt, Biotechnology grade) in the titrant solution was determined by refractometry, and the denaturant concentration after each titrant injection was calculated using the equations of Pace (*22*).

The chemical denaturation data were fit with the three-state model described above using an Igor Pro procedure (IgorDenat) where the fluorescence anisotropy was given by the weighted sum of three contributions:

$$F = \alpha_{N1}(A + B[\text{GdnHCl}]) + \alpha_{N2}(C + D[\text{GndHCl}]) + \alpha_{N3}(E + F[\text{GdnHCl}]) \quad (9)$$

where A, B, C, D, E, and F are the respective y-intercepts and slopes describing the denaturant dependence of the anisotropy of the three species, and [GdnHCl] is the guanidine hydrochloride concentration. The fraction of each of the three states, α, was calculated using eq 7. The value of ΔG for each transition as a function of denaturant concentration was defined using the linear extrapolation method (LEM):

$$\Delta G_{(i)} = \Delta G_{o(i)} + m[\text{GndHCl}] \quad (10)$$

The m-values were assumed to be identical for the two reactions. Denaturation data were obtained at different temperatures, and the data were globally fit to the integrated Gibbs−Helmholtz equation (eq 3) to obtain the thermodynamic parameters for the reactions. The fitted parameters in the global fit for the three-state model were the global m-value and ΔC_P, T_m, and ΔH for the first transition ($N_1 \leftrightarrow N_2$), T_o and ΔH_o for the second transition ($N_2 \leftrightarrow 2U$), and baseline parameters (slopes and y-intercepts) for each temperature (four for each data set since $C = A$ and $D = B$, see results).

Circular Dichroism. CD measurements were performed on an Olis (Bogart, GA) spectrometer equipped with a Peltier unit for temperature control. Experiments were performed in 0.1 and 1 cm path length cells in 10 mM glycine buffer with 50 mM KCl with pH ranging from 3 to 5. The secondary structure of the protein was determined using CDPro with a reference set of 48 proteins over a wavelength range of 190−240 nm (*23*).

NMR Spectroscopy. NMR spectra were collected on a Varian (Palo Alto, CA) 800 MHz (18.7 T field) INOVA NMR spectrometer using a triple resonance probe with triaxial pulsed field gradient capability and a Varian 500 MHz (11.7 T field) INOVA NMR spectrometer with z-axis pulsed field gradient capability. Pulse sequences were either those provided in the Varian (Palo Alto, CA) BioPack or

were kindly provided by Dr. Lewis Kay (University of Toronto). All NMR spectra were collected at 30 °C unless indicated otherwise. ^{1}H chemical shifts were referenced using sodium 4,4-dimethyl-4-silapentane-1-sulfonate (DSS) as an internal reference. ^{13}C and ^{15}N chemical shifts were referenced indirectly to DSS and liquid ammonia, respectively, using the appropriate frequency ratios (*24*). NMR spectra were processed using NMRPipe (*25*), FELIX (Accelrys, San Diego, CA), or VNMR (Varian, Palo Alto, CA). NMRView (*26*) was used for visualization and chemical shift assignments of NMR data.

NMR samples were prepared using lyophilized ^{15}N,^{13}C-enriched protein which was dissolved in 700 μL of 90% H_2O/10% D_2O or in 700 μL of 99.996% D_2O. Final protein concentrations were approximately 1 mM, and the pH was set to the desired value using a Radiometer glass electrode with either HCl or NaOH for 90% H_2O/10% D_2O solutions or DCl or KOD for 99.996% D_2O solutions. No correction was made for the deuterium isotope effect on pH. An NMR sample for a ^{12}C-filtered,^{13}C-edited NOESY spectrum was prepared by mixing equimolar amounts of ^{15}N,^{13}C doubly labeled and unlabeled Sso10b2. The mixture was denatured by incremental addition of 7.46 M GdnHCl to obtain a final GdnHCl concentration of 5.5 M. The sample was then extensively dialyzed against water for 48 h to remove the denaturant, followed by lyophilization, and then dissolution in 700 μL of 99.996% D_2O and adjustment of the pH to 5.0.

^{1}H-^{15}N residual dipolar coupling measurements were made at 18.7 T using partially aligned, ^{15}N-labeled protein in a liquid crystalline media of *n*-alkyl-poly(ethylene glycol) and hexanol (*27*). Samples were prepared in 90% H_2O/10% D_2O with 5% C12E5 (Sigma) with a C12E5/hexanol molar ratio (*r*) of 0.87. Spectra of unaligned samples were obtained at 30 °C on a sample that had been gently heated after storage at 4 °C, and spectra of partially aligned protein were obtained on the same sample at 30 °C after mixing. Single bond ^{1}H-^{15}N RDCs were obtained using ^{1}H,^{15}N HSQC-IPAP pulse sequence obtained from Dr. L. Kay (University of Toronto). Raw data sets contained 672 data points in the ^{1}H dimension and 256 increments in the ^{15}N dimension. Data were linear predicted by a factor of 2 in the ^{15}N dimension, and zero-filled to obtain 1024 × 1024 (^{1}H × ^{15}N) data points in the final spectrum. Residual dipolar couplings were extracted using in-house NMRView scripts.

{^{1}H}-^{15}N NOE and ^{15}N T_1 and $T_{1\rho}$ measurements were performed at 11.7 T using sensitivity-enhanced, gradient-selected HSQC pulse sequences (*28*, *29*). ^{1}H saturation for {^{1}H}-^{15}N NOEs was obtained using a series of 120° ^{1}H pulses with 5 ms separation. Saturation was performed for 5 s, with a total recycle delay of 10 s for both saturated and unsaturated experiments. Suppression of cross-correlation effects in ^{15}N $T_{1\rho}$ experiments was obtained using a train of phase-alternated, random length ^{1}H CW pulses applied during the ^{15}N spin lock (*29*). T_1 delay times were 0.10, 0.21, 0.33, 0.46, 0.61, 0.715, 0.95, 1.16, and 1.40 s. $T_{1\rho}$ delay times were 0.01, 0.02, 0.03, 0.04, 0.05, 0.06, 0.08, and 0.10 s. R_1 and $R_{1\rho}$ data were fit with the CURVEFIT module of MODELFREE (*30*). R_2 relaxation rates were calculated from $R_{1\rho}$ rates as described by Korzhnev et al. (*29*). Duplicate {^{1}H}-^{15}N NOE experiments and duplicates of ^{15}N T_1 and $T_{1\rho}$ experiments at three different delay times were used to estimate uncertainties in peak intensities. The errors in measured R_1, R_2, and NOE values averaged 0.8, 1.2, and 2.6%, respectively. The errors used for relaxation analysis were those measured or 2.5%, whichever was greater.

NMR Assignments. Backbone ^{1}H, ^{13}C, and ^{15}N assignments were obtained using ^{1}H-^{15}N heteronuclear single quantum coherence (HSQC), HNCA, HNCO, HNCACB, CBAC(CO)-NNH, HN(CO)CA, and HNHA spectra collected at 18.7 T on a uniformly ^{15}N,^{13}C-double-labeled protein sample dissolved in 90% H_2O/10% D_2O. Side chain assignments were obtained using HCC-TOCSY-NNH and CCC-TOCSY-NNH on an ^{15}N-^{13}C-labeled protein in 90% H_2O/10% D_2O, and HCCH-TOCSY and HCCH-COSY on a doubly labeled protein in 99.996% D_2O. A 3D HBGCBGCCBGCACONNH spectrum (*31*) of protein in 90% H_2O/10% D_2O was obtained for assignments of side-chain carboxyl carbons. HBCB-CGCDHD (*32*), 2D DQF-COSY, 2D NOESY, and ^{1}H,^{13}C HSQC spectra were collected on a doubly labeled protein sample in 90% H_2O/10% D_2O to obtain aromatic proton and carbon assignments. An ^{15}N-edited nuclear Overhauser effect spectrum (NOESY) (150 ms mixing time) on doubly labeled protein in 90% H_2O/10% D_2O and a NOESY-^{13}C HSQC experiment (150 ms mixing time) on protein in 99.996% D_2O were collected for NOE measurements. For intermolecular NOE assignments, a 3D ^{12}C-filtered, ^{13}C-edited NOESY NMR experiment (*33*) (150 ms mixing time) in 99.996% D_2O was performed at 18.7 T on a sample of hetero-labeled dimer prepared as described above. Backbone amide protons involved in hydrogen bonding were delineated with a ^{1}H,^{15}N HSQC spectrum of ^{15}N-labeled protein immediately after dissolving in 99.996% D_2O.

NMR Structure Calculation. Initial structures of monomeric Sso10b2 were derived using ARIA 1.2 interfaced to CNS (*34*) with a random chain starting structure. Initial restraints consisted of hydrogen bond and dihedral angle restraints, obtained from chemical shift indices, and a set of unambiguous NOEs, obtained from an ^{15}N-edited NOESY spectrum. In each ARIA iteration, distance restraints were calibrated and NOE assignments of the ^{15}N-edited NOESY cross-peaks were made by ARIA based on an ensemble of the lowest energy structures from the previous iteration. Assignments made by ARIA were checked manually, as were the distance restraints rejected by ARIA. Once a preliminary monomer structure with reasonable convergence was obtained, NOEs from a ^{13}C-edited NOESY spectrum were incorporated and assigned by ARIA. The final ensemble of monomeric structures was validated using PROCHECK. The average monomer structure was calculated using the 10 best structures and then energy-minimized in CNS. A simulated annealing protocol was used to generate 100 more monomer structures in CNS, starting with the average minimized structure and final distance restraints obtained from ARIA. A ^{12}C-filtered, ^{13}C-edited NOESY experiment was used to identify a set of 22 unambiguous intermolecular NOE assignments which were used to dock two monomers to form a starting dimer structure. Structure calculations for the dimer were performed using ARIA1.2 modified for homodimers (B. Jordan, personal communication). NOEs from ^{15}N-edited NOESY, ^{13}C-edited NOESY, and ^{13}C-filtered, ^{12}C-edited NOESY spectra were included in refinement of the dimer along with hydrogen bond distance restraints (33 per monomer) obtained from hydrogen−deuterium exchange

Table 1: Thermodynamic Parameters Obtained by DSC Describing Thermotropic Transitions in Sso10b2 as a Function of pH and Concentration[a]

		transition 1				transition 2			
pH	concentrated (mg/mL)	T_m (°C)	ΔH_{vh} (kcal/mol)	ΔH_{cal} (kcal/mol)	$\Delta H_{cal}/\Delta H_{vh}$	T_O (°C)	ΔH_{vh} (kcal/mol)	ΔH_{cal} (kcal/mol)	$\Delta H_{cal}/\Delta H_{vh}$
3.2	1.0	57.8 ± 0.1	39.1 ± 0.1	20.3 ± 0.1	0.520 ± 0.007	93.4 ± 0.2	85.5 ± 0.3	42.8 ± 0.2	0.501 ± 0.007
4.2	1.0	81.1 ± 0.1	60.0 ± 0.2	30.1 ± 0.1	0.501 ± 0.005	115.6 ± 0.2	93.5 ± 0.2	47.8 ± 0.1	0.511 ± 0.005
4.8	1.0	86.5 ± 0.1	75.5 ± 0.2	37.8 ± 0.1	0.501 ± 0.004	126.2 ± 0.1	92.7 ± 0.2	47.3 ± 0.1	0.510 ± 0.006
5.6	1.0	88.1 ± 0.1	95.5 ± 0.3	44.8 ± 0.1	0.469 ± 0.005	130.9 ± 0.2	105.0 ± 0.5	56.9 ± 0.3	0.542 ± 0.010
6.0	0.5	88.4 ± 0.1	88.1 ± 0.4	43.8 ± 0.2	0.497 ± 0.005	128.6 ± 0.1	104.0 ± 0.2	51.8 ± 0.1	0.498 ± 0.008
6.0	1.0	88.1 ± 0.1	97.0 ± 0.3	46.1 ± 0.1	0.475 ± 0.004	131.1 ± 0.2	106.1 ± 0.4	57.0 ± 0.2	0.537 ± 0.009
6.0	1.4	87.8 ± 0.1	101.7 ± 0.3	46.9 ± 0.1	0.461 ± 0.005	132.5 ± 0.3	103.4 ± 0.8	58.1 ± 0.4	0.562 ± 0.012
6.0	2.0	87.7 ± 0.1	106.0 ± 0.4	46.4 ± 0.2	0.438 ± 0.007	134.6 ± 0.4	99.1 ± 1.0	59.5 ± 0.6	0.600 ± 0.017
6.0	2.6	87.5 ± 0.1	111.2 ± 0.5	46.3 ± 0.2	0.416 ± 0.007	135.9 ± 0.4	98.6 ± 0.7	50.3 ± 0.4	0.510 ± 0.003
7.1	1.0	88.3 ± 0.1	171.8 ± 1.3	27.0 ± 0.2	0.157 ± 0.002	157.4 ± 1.1	84.7 ± 1.5	44.9 ± 0.8	0.530 ± 0.028

[a] Parameters were obtained from fitting the DSC data shown in Figure 2 using the three-state unfolding model as described in the text. All data were collected in 10 mM glycine at the indicated pH and protein concentrations.

data. Residual dipolar couplings (81 per monomer) were included as restraints using initial values for D_a and R of 10.0 and 0.53, calculated from the starting dimer structure using MODULE.

The dimer structure was further refined using Xplor-NIH (*35*) (version 2.11) with the distance restraints derived by ARIA from the NOE cross-peaks. Restraints are summarized in Table 2. T_1 and T_2 relaxation data restraints were those that did not fall in suspected mobile regions, which were identified by significantly low {^{1}H}-^{15}N NOEs. Xplor-NIH internal dynamics were used with an initial equilibration at 3000 K, slow cooling to 100 K with 50 K temperature decrements, followed by energy minimization. During both the equilibration and cooling phases, distance restraint force constants were increased from 5 to 50 kcal/mol, and force constants for dipolar coupling and T_1/T_2 restraints were increased during the cooling phase from 0.01 to 1.0 and from 0.05 to 5.0, respectively. A grid search with rigid body rotation was implemented at each temperature change during the simulated annealing to find optimal values of D_a, $D_{\parallel}/D_{\perp}$, R (rhombicity), and the overall rotational correlation time. The final values characterizing the molecular alignment tensor were a D_a of 9.1 Hz and a rhombicity of 0.56. The rotational diffusion anisotropy defined by the T_1/T_2 restraints converged to a $D_{\parallel}/D_{\perp}$ of 1.4 with a rhombicity of 0.03 and an overall τ_m of 17.8 ns.

The 10 lowest energy structures from Xplor-NIH refinements (out of 100 total structures) were used to define an ensemble of NMR structures, and an average structure was obtained by averaging the coordinates followed by restrained energy minimization. The quality of the final structures were analyzed using PROCHECK-NMR. The coordinates and resonance assignments have been deposited in the Protein Data Bank (PDB: 2A2Y) and the BioMagResBank (BMRB 5891).

{^{1}H}-^{15}N NOE and ^{15}N Relaxation Data Analysis. {^{1}H}-^{15}N NOE and ^{15}N R_1 and R_2 relaxation data were analyzed using TENSOR2 kindly provided by M. Blackledge (http://www.ibs.fr/ext/labos/LRMN/softs/). The diffusion tensor elements were calculated using data for NHs only in α or β secondary structures with NOEs greater than 0.7, R_2 values greater than 20 s^{-1}, and R_2/R_1 ratios within 1 standard deviation of the mean. The principal elements of the diffusion tensor elements were as follows: $D_x = 0.86 \times 10^7$ s^{-1}, $D_y = 0.87 \times 10^7$ s^{-1}, and $D_z = 1.05 \times 10^7$ s^{-1}. Similar results were obtained using the quadric_diffusion program kindly provided by A. Palmer (Columbia University). The backbone dynamic parameters were obtained by fitting the ^{15}N relaxation data according to the "model-free" approach of Lipari and Szabo using an anisotropic model with TENSOR2.

Nucleic Acid Binding. Yeast RNA (Sigma, Type XI) was purified by phenol−chloroform extraction followed by

Table 2: Structural Statistics for the Sso10b2 Dimer

Number of experimental restraints[a]	
unambiguous NOE distances	1223
intraresidue	299
sequential residues	316
short and medium range	270
long range	225
intermolecular	110
ambiguous NOE distances	1651
H-bonds[b]	33
dihedral angle restraints[c]	126
$^3J_{HNH\alpha}$ coupling constants	48
residual dipolar couplings	80
T_1/T_2 relaxation ratios	57
coordinate rmsd[d]	
backbone (secondary structure only) (Å)	0.27
backbone (all residues) (Å)	0.48
all heavy atoms (Å)	0.95
number of restraint violations	
NOE distances with violations >0.5 Å	0.4
dihedral angles with violations >10°	0.6
rmsd of restraint violations	
distance restraints (Å)	0.005
dihedral angles (deg)	1.40
$^3J_{HNH\alpha}$ (Hz)	1.49
residual dipolar couplings (Hz)	1.00
T_1/T_2 relaxation ratios	0.78
rmsd from ideal geometry	
bonds (Å)	0.004
angles (deg)	0.60
impropers (deg)	0.60
Ramachandran plot statistics	
most favored (%)	86.7
allowed (%)	10.6
generously allowed (%)	2.5
disallowed (%)	0.2

[a] Number of final restraints used for Xplor-NIH refinement given per monomer. [b] Each of the 33 H-bonds was defined by two restraints: the H−O and N− O distances. [c] Phi and psi dihedral angles were derived from the CSI. [d] Coordinate rmsd values were determined by superposition of the 10 best Xplor-NIH structures over the residues which occur in well-ordered regions where the local rmsd was less than the mean rmsd + 2 standard deviations (residues 6, 7, 9−12, 16−28, 31−54, 58, 60−63, 65−70, and 78−88).

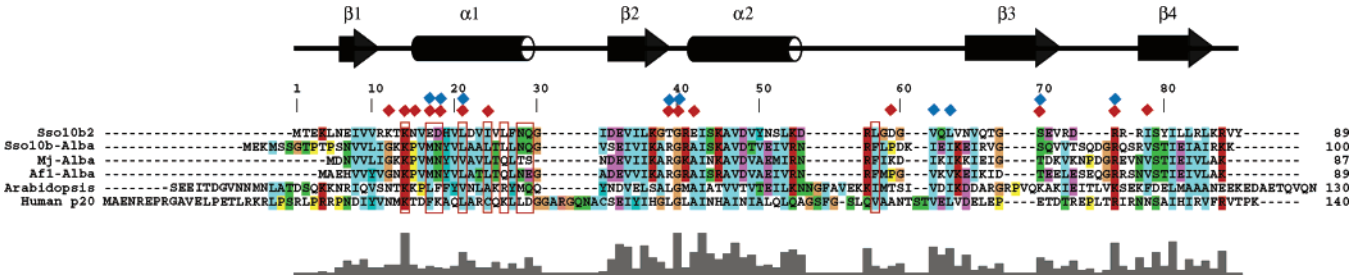

FIGURE 1: Sso10b2 (accession Q97ZF4) primary and secondary structure with sequence alignments with Sso10b (Alba) (P60849), Af1-Alba from *Archaeoglobus fulgidus* (O28323), Mf1-Alba from *Methanococcus jannaschii* (Q57665), an unnamed gene product from *Arabidopsis thaliana* (BAC42164), and p20 from *Homo sapiens* (O75817). Numbering above the sequences is for Sso10b2. The Sso10b2 residues showing ^{1}H,^{15}N HSQC chemical shift perturbations due to yeast RNA and single-stranded *E. coli* DNA binding are marked with red and blue diamonds, respectively. Residues shown to be involved in protein−protein interactions via interface II (*15*) are outlined with red boxes surrounding Sso10b2 and homologous residues. The level of sequence homology is indicated by the bar chart below the sequences as well as with color highlighting using the ClustalX default parameters (red, 60% K and R; purple, 50% D and E; light blue, 60% hydrophobic; green, 80% uncharged hydrophilic; all P and G are orange).

ethanol precipitation. The precipitated RNA was suspended in 10 mM KH_2PO_4 buffer and the pH adjusted to 7.0. All glassware used in RNA experiments was heated to 150 °C for approximately 12 h. In addition, all glassware and plasticware were washed with DEPC-treated water. *E. coli* DNA (Sigma) was used for double-stranded DNA titrations without further purification and was sheared by passing through a 26 gauge needle. Single-stranded DNA was made by heating *E. coli* DNA through the melting transition (monitored by UV absorbance) and then rapidly cooling the sample to 0 °C.

RNA and DNA titrations followed by fluorescence were performed on a Fluoromax-3 fluorimeter (Jobin Yvon, Inc.) with excitation at 275 nm and emission at 303 nm (4 nm slit widths). Reverse titrations (nucleic acid into protein) were performed by adding 3 μL of 2.3 mM nucleic acid solution (in 10 mM KH_2PO_4, pH 7.0, 20 °C) to 2.5 mL of protein solution (same buffer with 2.9 μM protein monomer) in a 4 mL quartz fluorescence cell. Binding parameters were obtained by using the McGhee−von Hippel model for nonspecific ligand binding to an infinite lattice (*36*).

Nucleic acid titrations followed by NMR were performed using ^{1}H,^{15}N HSQC spectra of ^{15}N-labeled Sso10b2. Reverse titrations were performed by adding aliquots of a concentrated nucleic acid solution in 10 mM KH_2PO_4 (pH 7.0) into 0.2 mM protein in the same buffer with 90% H_2O/10%D_2O at 30 °C. Single-stranded DNA titrations were performed in the same buffer with 0.3 M KCl to reduce precipitation and promote fast exchange. Changes in ^{1}H,^{15}N HSQC spectra were quantified using the length of the vector describing the chemical shift change for each peak

$$\Delta\delta = \sqrt{(\Delta\delta_{HN})^2 + (0.15\Delta\delta_N)^2} \qquad (11)$$

where the weighting factor 0.15 is determined by the relative magnitudes of the amide nitrogen chemical shift range compared to that for the NH proton chemical shift range (*37*).

RESULTS

Initial Characterization of Sso10b2. The *S. solfataricus* genome (*38*) contains two annotated Sso10b genes: P60849 (locus tag SSO0962) and Q97ZF4 (SSO6877). The protein coded by the first has been the most studied and corresponds to Sso10b or Alba (*13*). Q97ZF4 codes for Sso10b2 (*14*), a highly basic 10 239 Da (89 residue) protein with a calculated pI of 9.39 (compared to 10.48 for Sso10b) and 36% sequence identity to Sso10b (Figure 1). The Sso10b2 gene was cloned and expressed as described in Materials and Methods. Sso10b2 contains no tryptophan (and three tyrosines), leading to a relatively low near-UV absorbance with an extinction coefficient of 0.38 mL/(cm·gm) at 280 nm.

Dimerization in Solution. Gel filtration chromatography of recombinant protein showed an apparent molecular weight of 17 000, indicating dimer formation in solution (in 10 mM KH_2PO_4 and 0.15 M KCl, pH 7). A van Holde−Weischet analysis (*39*) of sedimentation velocity data indicated the presence of a single Sso10b2 species in 10 mM KH_2PO_4 and 0.15 M KCl, pH 7. Fitting of the sedimentation profiles indicated a sedimentation coefficient, $S_{20,w}$, of 1.96 ± 0.01 and a mass of 20 000 ± 500, consistent with an Sso10b2 dimer. The frictional coefficient relative to that of a sphere of the same mass (f/f_o) was 1.16, which indicated a nearly spherical globular dimer.

Thermal Stability. Since Sso10b2 is a hyperthermophile protein, it is of interest to characterize the effect of temperature on the structure and oligomerization properties of the protein, especially near the growth temperature (80 °C). Sso10b2 was shown to be thermally stable by DSC, with a T_m greater than 85 °C above pH 5 with 1 mg/mL Sso10b2 (Figure 2). Thermal unfolding was reversible from pH 3 to 7 in 10 mM glycine as demonstrated by heating to the midpoint temperature, cooling, and rescanning to 125 °C (data not shown). Reversibility was reduced in 50 mM KCl at higher pH.

The DSC profile for Sso10b2 varied with protein concentration as expected for an oligomer. Surprisingly, two significant endotherms were observed above pH 5 with protein concentrations greater than 1 mg/mL (Figure 2). Variation of protein concentration resulted in no change in the T_m of the first transition (T_m = 88 °C), while the T_m of the second increased with increasing protein concentration at pH 6.0 (Figure 2B). (The intracellular pH of *Sulfolobus* is approximately 6.0 (*40*).) The lack of a concentration dependence for the low-temperature endotherm indicated that this reflected a structural transition without a change in the number of species, and it was presumed to be a dimer ↔ dimer transition (at pH 6.0). The concentration dependence of the second (higher temperature) endotherm demonstrated that it corresponded to an increase in the number of molecular

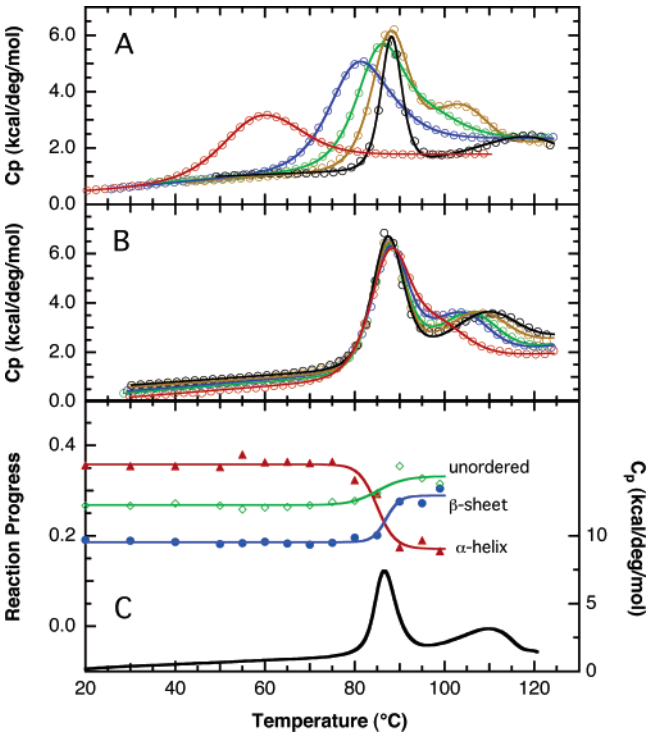

FIGURE 2: Thermal unfolding of Sso10b2 as a function of pH and protein concentration. (A) DSC of Sso10b2 (1 mg/mL) in 10 mM glycine at pH 3.2 (red), 4.2 (blue), 4.8 (green), 5.6 (brown), and 7.1 (black). (B) DSC of Sso10b2 in 10 mM glycine, pH 6.0, collected at protein concentrations of 0.5 (red), 1.0 (blue), 1.4 (green), 2.0 (brown), and 2.6 (black) mg/mL. The symbols represent data (for clarity only every fifth data point is shown), and solid lines represent fits of the data using the three-state model discussed in the text. The fitted parameters are given in Table 1. (C) Temperature dependence of the secondary structure of Sso10b2. Circular dichroism spectra of Sso10b2 (0.1 mg/mL in 10 mM glycine (pH 5) and 50 mM KCl) from 20 to 99 °C were analyzed using CDPro to define the change in secondary structure with temperature. A DSC scan of Sso10b2 (1 mg/mL, in the same buffer) is shown at the bottom of the panel.

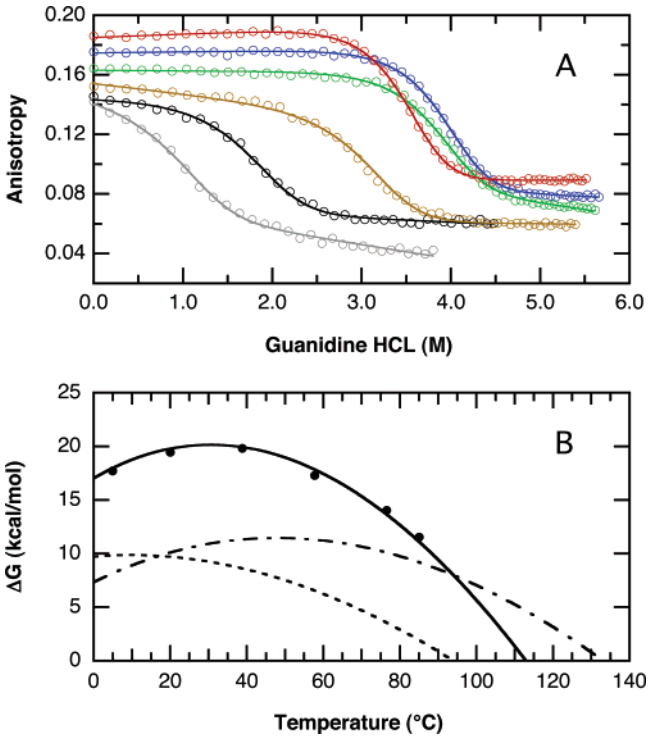

FIGURE 3: Chemical denaturation of Sso10b2 as a function of temperature. (A) Guanidine hydrochloride-induced unfolding of Sso10b2 in 10mM MOPS (pH 7.0) monitored by fluorescence anisotropy at 5.0 (red), 20 (blue), 39 (green), 58 (brown), 77 (black), and 85 (gray) °C. Solid lines represent the global fit of all the data to the integrated Gibbs−Helmholtz equation (eq 3) using the three-state model described in the text. Fitted parameters are $\Delta C_p = 1961$ cal deg^{-1} mol^{-1}, m-value = 1660, $T_m = 94$ °C, $\Delta H_{vh} = 82.4$ kcal/mol, $T_o = 133.1$ °C, and $\Delta H_o = 105.1$ kcal/mol. (B) Stability curves for the $N_1 \leftrightarrow N_2$ (short dashes), $N_2 \leftrightarrow 2U$ (long dashes), and $N_1 \leftrightarrow 2U$ (solid line) transitions defined by the fitted parameters. Symbols indicate the individually calculated ΔG values determined by fitting the data to a global m-value using a two-state ($N_1 \leftrightarrow 2U$) dimer unfolding model and are shown for comparison only.

species, which was presumed to be unfolding and dissociation of the dimer under these conditions. The data can be explained by a three-state model (see Materials and Methods) with a transition between two dimeric forms which can dissociate and unfold to two random coil chains. Nonlinear fitting of the DSC data to the model provided transition temperatures (T_m for the first, T_o for the second) and enthalpies (ΔH_{vh} and ΔH_{cal}) for the two endotherms (Table 1). Both endotherms were pH-dependent, with the higher temperature endotherm showing a greater dependence on pH above pH 5, while the lower temperature endotherm shifted significantly to lower temperature below pH 5. Below pH 5, the two endotherms appeared to coalesce into a single peak as the pH decreased. All of the data could be fit globally with the three-state model. At pH 3.2, the T_m of the single peak was concentration-dependent, indicating contributions from dimer unfolding as expected for the three-state model.

Below pH 7, the $\Delta H_{cal}/\Delta H_{vh}$ ratio was about 0.5 for both transitions, as expected for a dimer. However, at pH 7 and above, the cooperativity of the first transition increased (i.e., $\Delta H_{cal}/\Delta H_{vh}$ was less than 0.5), suggesting that the lower temperature endotherm represented a structural transition involving higher order oligomers (i.e., larger than dimers). The T_m of the transition remained concentration-independent, indicating that the first transition corresponded to a structural rearrangement or partial unfolding without dissociation. There was little change in the $\Delta H_{cal}/\Delta H_{vh}$ ratio for the second higher temperature transition as a function of pH.

Chemical Denaturation. Although DSC of Sso10b2 showed two thermotropic transitions at pH 7, only one unfolding transition was apparent in guanidine hydrochloride titrations of Sso10b2 at pH 7.0 between 5 and 85 °C as monitored by fluorescence anisotropy (Figure 3). Therefore, either the dimer−dimer transition observed by DSC resulted in no change in protein anisotropy (and was therefore not directly measurable) or one of the dimeric states was not significantly populated during chemical denaturation (so that only $N_1 \leftrightarrow 2U$ or $N_2 \leftrightarrow 2U$ could be observed). Simulations using the three-state model with the thermodynamic parameters determined by DSC indicate that N_2 is expected to be minimally populated (less than 1%) below 40 °C. The population of N_2 increases with increasing temperature and approaches 25% at 85 °C. Since there is only one observable transition at high temperature, any anisotropy change associated with the $N_1 \leftrightarrow N_2$ transition must be negligible. Therefore, we have fit the chemical denaturation data with the three-state model assuming that the $N_1 \leftrightarrow N_2$ transition makes no contribution to the observed signal (i.e., $C = A$ and $D = B$ in eq 9). Note that although the $N_1 \leftrightarrow N_2$ transition is not

directly observable by fluorescence anisotropy, this transition has a significant influence on the population of unfolded species and therefore is observable thermodynamically. A global fit of the denaturation data to the Gibbs−Helmholtz equation gave a ΔC_P of 1961 ± 50 cal deg^{-1} mol^{-1}, along with a T_m of 94.0 ± 1.4 °C, a ΔH = 82.4 ± 5.7 kcal/mol for the dimer $N_1 \leftrightarrow N_2$ transition, a T_o of 133.1 ± 4.8 °C and ΔH_o of 105.1 ± 5.6 kcal/mol for the $N_2 \leftrightarrow 2U$ unfolding transition, and an *m*-value of 1660 ± 33. These parameters are in good agreement with those obtained from an analysis of the DSC data (Figure 2). Both chemical denaturation and DSC parameters indicate that the $N_1 \leftrightarrow N_2$ transition occurs first with increasing temperature (at pH 7), followed by the unfolding transition $N_2 \leftrightarrow 2U$. Increasing denaturant at low temperature (e.g., 25 °C) leads to direct conversion of $N_1 \leftrightarrow 2U$ without formation of the second dimeric form N_2. The second dimeric form is only populated at high temperature near the growth temperature of *Sulfolobus* (i.e., 80 °C).

Circular Dichroism Analysis of Thermal Transitions. Analysis of CD spectra of Sso10b2 collected at 20 °C (pH 5) showed that the protein consisted of approximately 35% α-helix, 20% β-sheet, and 45% turns and others structures. Data collected at higher temperatures showed that the secondary structure of the protein changed significantly near 85 °C (Figure 2C). A transition in the CD at this temperature showed an increase in β-sheet from 20% to approximately 30%, while the α-helical content decreased from 35% to approximately 15%. A DSC scan under similar conditions showed that this transition coincided with the first endotherm in DSC scans. Thus, the concentration-independent transition observed in DSC corresponds to a partial unfolding along with an increase in β-sheet without dissociation of the dimer.

NMR Spectroscopy and Structure Calculation. The ^{1}H,^{15}N HSQC spectrum of Sso10b2 at pH 4.8 and 30 °C showed excellent chemical shift dispersion with 87 cross-peaks (Figure 4). There was no evidence of two protein conformations as observed in the NMR spectra of Ssh10b (*41*). Two conformations of Ssh10b were shown to be due to cis−trans isomerization of the L61−P62 peptide bond in that protein. The lack of two conformations in Sso10b2 under similar conditions is consistent with the occurrence of an aspartate at the corresponding position (D59) in Sso10b2. This greatly facilitates chemical shift assignments and structure determination. Backbone ^{1}H, ^{15}N, and ^{13}C assignments were obtained for all residues in Sso10b2 beyond threonine-2 (see Materials and Methods), and more than 90% of the side-chain protons and carbons were assigned. The assignment data indicated that the initiating methionine was absent in the recombinant protein.

NMR solution structures of Sso10b2 were obtained using NOE, CSI, dihedral angle, hydrogen bond, RDC, and ^{15}N relaxation data restraints from data collected at 30 °C. A superposition of the 10 lowest energy structures is shown in Figure 5, with a summary of the structural statistics in Table 2. A Ramachandran plot (not shown) of the backbone dihedral angles of the ensemble indicated convergence to good stereochemistry. The ensemble of the 10 best structures showed an average backbone rmsd on the order of 0.25 Å (Figure 6), with slight increases approaching 0.5 Å at the connecting elements between regular secondary structure. The largest backbone rmsd was noted at the N-terminus.

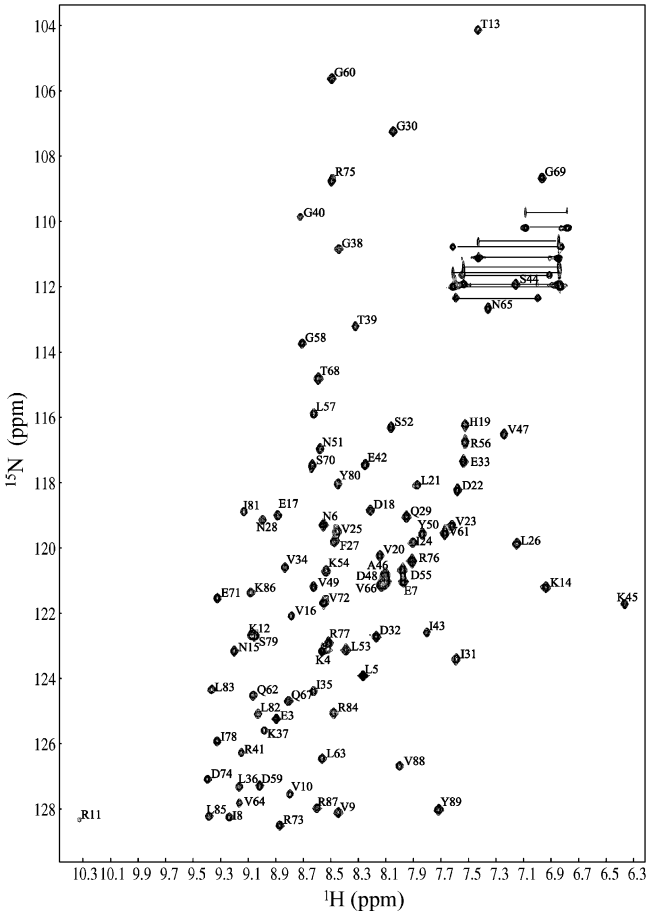

FIGURE 4: ^{1}H,^{15}N HSQC spectrum of Sso10b2 in 90% H_2O/10% D_2O (pH 4.8) collected at 30 °C and at 18.7 T. The asparagine and glutamine side-chain correlation peaks are connected with solid lines.

The solution structure of Sso10b2 contains 39% β-sheet, 31% α-helix, and 30% of other structure, with two parallel α-helices and four β-strands arranged to form a $\beta_1\alpha_1\beta_2\alpha_2\beta_3\beta_4$ topology (Figure 5). After the first five N-terminal residues, the structure begins with a short β-strand (β1, N6−V9), followed by a loop of six residues (V10−N15) connecting to the first helix α_1. This loop is positively charged with one arginine (R11) and two lysine (K12 and K14) residues. K14 is homologous to the lysine shown to be specifically acetylated in Alba (*4*). Helix α_1 (V16−Q29) is especially interesting because of the predominance of hydrophobic (V16, V20, L21, V23, I24, V25, L26, and F27) and negatively charged (E17, D18, and D22) residues. There are no positively charged residues in this helix other than potentially H19, which is largely buried with a hydrogen bond to the NH of R11 (leading to a significant downfield shift of the both the ^{1}H and ^{15}N resonances). The second β-strand (E33−T39), which follows, ends in an unusually tight turn containing a highly conserved G40 as well as R41 (Figure 1). These are immediately followed by α_2 (E42−K54), which is largely buried and contributes to the hydrophobic core of the monomer as well as the hydrophobic interface between two monomer units in the dimer. The sequence ends with two antiparallel β-strands (β_3, V66−V72 and β_4, R77−K86) forming a β-hairpin "arm" which extends beyond the body of the monomer. The turn at the end of the arm is a short loop (R73−R76) which contains an arginine-rich sequence (RDRRR) commonly associated

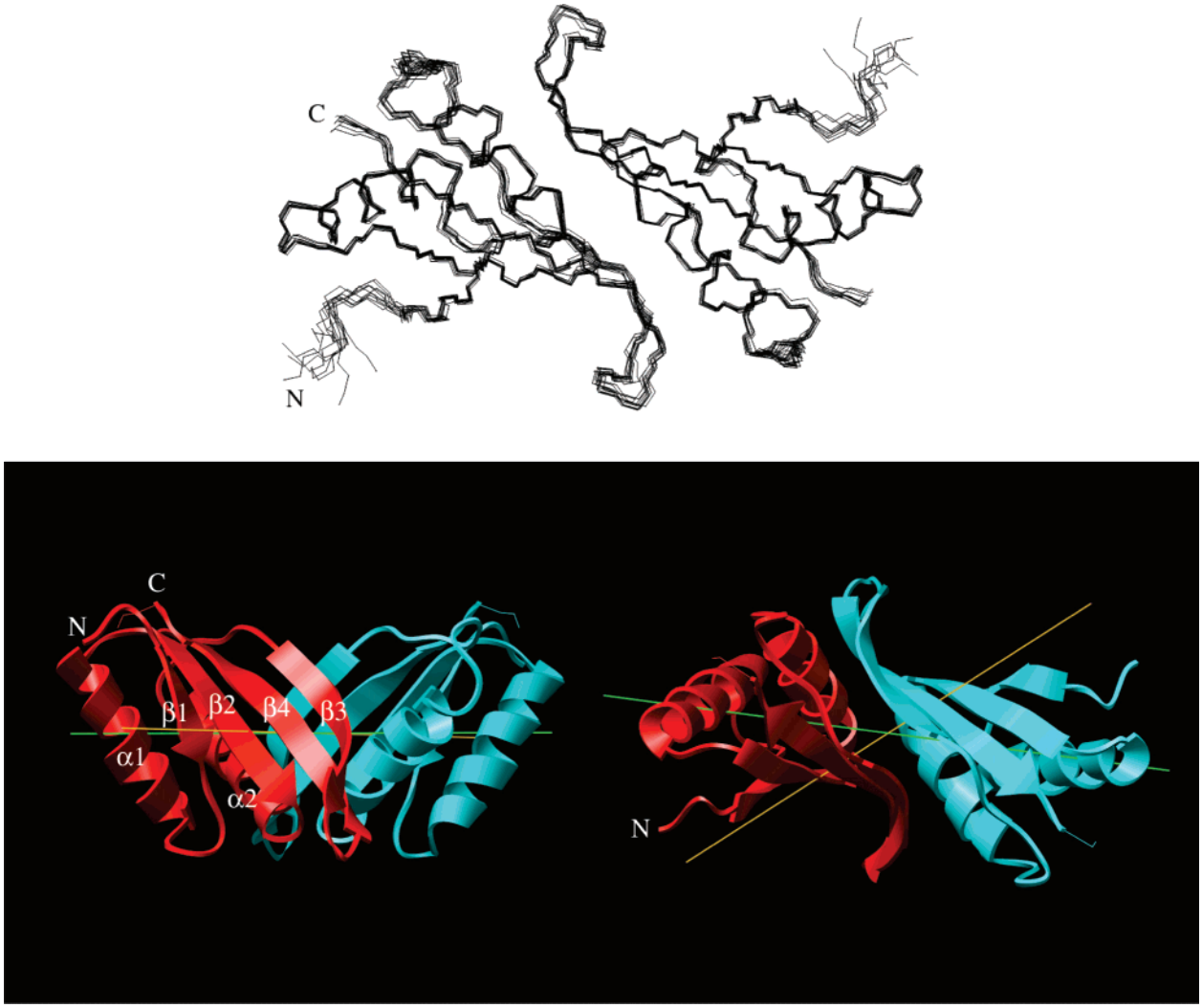

FIGURE 5: The structure of Sso10b2. (Upper panel) An overlay of the ensemble of 10 lowest energy NMR solution structures of Sso10b2. The N- and C-termini are indicated for one of the monomers. (Lower panel) The solution structure of dimeric Sso10b2 shown as ribbon diagrams in two different orientations. The monomers in each view are indicated in blue and red. The *z*-axes of the diffusion and alignment tensors are indicated by green and gold lines, respectively. The numbering of the helices and β-strands is indicated for one monomer in the left view.

with RNA binding (*14*, *42*). The arm is oriented away from the dimer and is expected to be important in nucleic acid binding (see below).

Dimerization of Sso10b2 in solution occurs at a hydrophobic surface on the C-terminal α_2-β_3-β_4 segments defined by I43, V47, L63, V66, I81, and L83. In addition, polar side chains from S44, T68, S70, and S79 also contribute to the dimerization surface, with potential H-bonding between T68 and Y50. Interestingly, there is little evidence for ion pairing between subunits. The only possible pairs involve R77, D48, and D55, but the separation distances (greater than 6 Å) make these unlikely to be important in stabilizing the dimer. The pH dependence noted for the dimer dissociation (the second, higher temperature transition) observed by DSC occurs over a range consistent with histidine titration (i.e., pH > 6). However, the only histidine (H19) is largely buried in the hydrophobic core of the monomers and is not at the dimer interface (Figure 7).

Sso10b2 contains a significant charge density with 16 positively (9 arginines, 7 lysines) and 13 negatively (7 aspartate and 6 glutamate) charged residues. Potential salt-bridges involving residues E7−K37, K4−D32, E33−R84, E42−R73, and K14−E18 could be identified in the final structures. The charges are not uniformly positioned on the surface (Figure 7) so that a high density of positive charge occurs on the face defined by the loops at the C-terminal ends of β-strands β_1, β_2, and β_3. Interestingly, K14 (homologous to the acetylated lysine in Alba) lies at the edge of this face, and H19 is nearby.

^{15}N relaxation rates and NOEs indicate a region of significant flexibility around residues 70−78 (Figure 6), corresponding to the arginine-rich arm that presumably is involved in nucleic acid binding (see below). This region also exhibits an increased rmsd in the backbone atoms of the ensemble of the 10 best structures. Except for another small region of increased flexibility toward the C-terminus of helix 2 (residues 53−56), the remainder of the protein appears relatively rigid with a mean S^2 value of 0.95.

Nucleic Acid Binding. RNA and DNA binding to Sso10b2 resulted in quenching of the intrinsic tyrosine fluorescence (the protein contains no tryptophan). Reverse titrations of nucleic acid into Sso10b2 showed a typical rectangular hyperbola with maximal quenching of approximately 40% in 10 mM KH_2PO_4 (pH 7, 20 °C). The binding isotherm

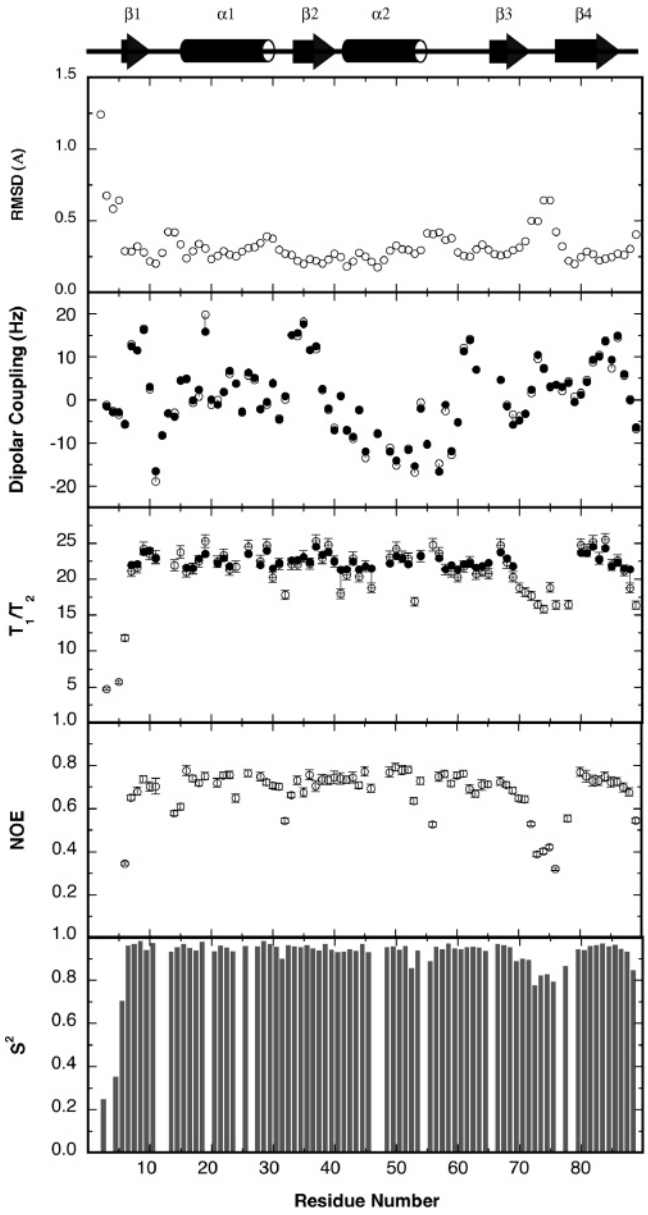

FIGURE 6: Sequence-dependent properties of Sso10b2. (A) Average backbone rmsd of the 10 best (lowest energy) structures relative to the average structure calculated from the 10 structures. (B) Experimental NH residual dipolar couplings (○) compared to those calculated from the average structure (●). (C) Experimental ^{15}N T_1/T_2 ratios (±1 standard deviation) (○) compared to those calculated using the average structure (●). Calculated values are only shown for those used in the structure refinement. (D) Measured $\{^1H\}^{15}N$ NOEs (±1 standard deviation) (E) Generalized order parameters (S^2) of NH vectors calculated from ^{15}N relaxation data.

could be fit by the McGhee−von Hipple model (*36*) for nonspecific binding to an infinite lattice. The protein showed a relatively high affinity for single-stranded *E. coli* DNA with a K_d of 2.6×10^{-7} M and a site size of 3.7 bases per dimer (Figure 7). Titrations with double-stranded *E. coli* DNA indicated significantly weaker binding ($K_d = 1.5 \times 10^{-5}$ M) with a site size of 5.6 base pairs per dimer. The affinity for yeast RNA was weaker than for single-stranded DNA at approximately 1.3×10^{-6} M and a binding site size of 5.1 bases per dimer.

An indication of the Sso10b2 residues contributing to the nucleic acid binding site was obtained by chemical shift perturbation of $^1H,^{15}N$ HSQC spectra of the protein by single-stranded DNA and RNA. RNA binding resulted in NH chemical shift perturbations for residues on the surface defined by the C-termini of the α_1 helix and the β_1, β_2, and β_3 strands (viz., K12, K14, N15, E17, D18, L21, I24, T39, G40, E42, S70, R75, and I78) (red diamonds, Figure 1). At the concentrations needed for NMR, the addition of single-stranded *E. coli* DNA to Sso10b2 led to precipitation of the complex with no noticeable change in the NMR spectrum of the protein remaining in solution. Precipitation was not observed in the presence of 0.3 M KCl, and at the higher salt concentration, single-stranded DNA led to perturbation of a subset of the NHs perturbed by RNA: E17, D18, L21, T39, G40, S70, and R75 (blue diamonds, Figure 1). These include residues at the surface defined by the C-termini of the β_1, β_2, and β_3 strands. In addition, these also include residues on the surface of the α_1-helix which coincide with those reported by Bell et al. (*4*) to be involved in protein−protein interactions at interface II (red boxes, Figure 1).

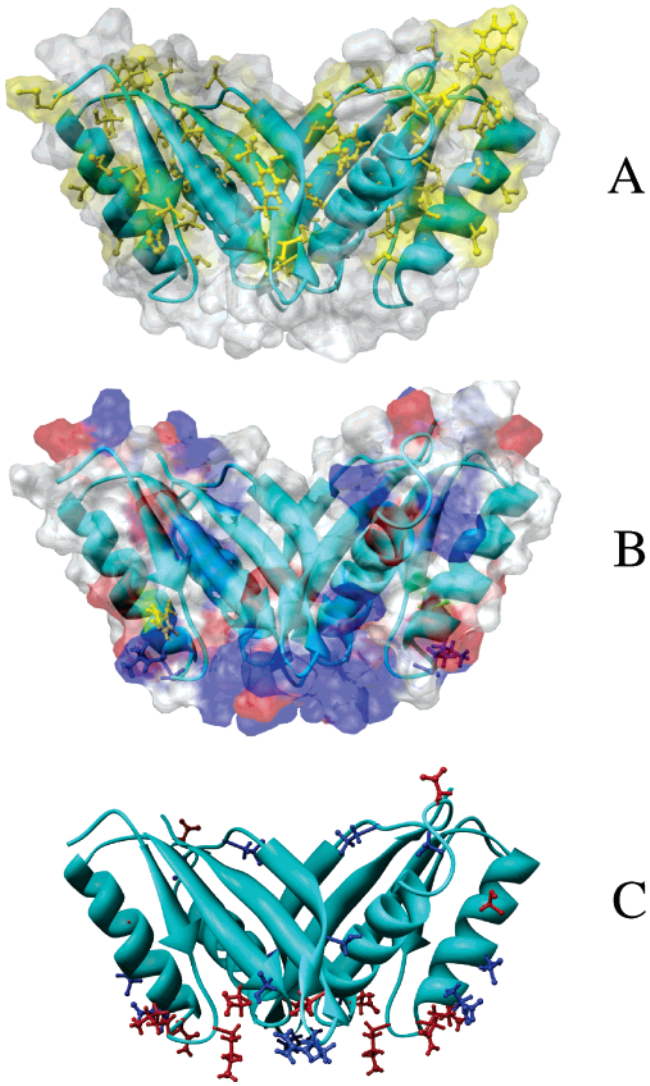

FIGURE 7: Distribution of hydrophobic, charged, and nucleic acid binding residues in dimeric Sso10b2. Hydrophobic residues are colored yellow in (A), and positively charged residues are colored blue, and negatively charged residues are shown in red in (B). H19 is indicated in yellow in panel B. (C) Sso10b2 residues with perturbed $^1H,^{15}N$ HSQC cross-peaks due to single-stranded *E. coli* DNA binding are indicated in blue, and additional residues perturbed by yeast RNA are shown in red.

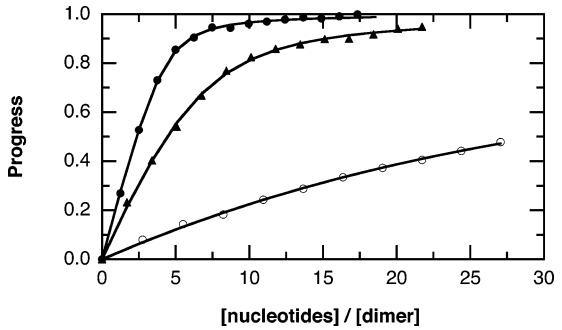

FIGURE 8: Nucleic acid binding by Sso10b2. Reverse titrations of Sso10b2 in 0.01 M KH2PO4 buffer (pH 7, 20 °C) with double-stranded *E. coli* DNA (○), single-stranded *E. coli* DNA (●), and yeast RNA (▲) monitored by fluorescence. Details are provided in the Materials and Methods. The solid lines are the best fits of the data using the McGhee−von Hippple model for nonspecific binding to an infinite lattice.

Interestingly, RNA perturbed D59 in the loop before the β_3 strand, while DNA perturbed the nearby V61 and L63.

DISCUSSION

Sso10b2 has been shown to be a highly stable and well-behaved member of the Alba family of proteins that is amenable to NMR structural studies as well as biophysical characterization of solution properties. The conformational heterogeneity previously described in NMR studies of the homologous Ssh10b (*41*) was not observed for Sso10b2. A temperature-dependent conformational transition in Ssh10b (from 10 to 60 °C) has been shown to be due to cis−trans isomerization of the L61−P62 peptide bond in that protein (*41*). Comparable behavior is expected for Sso10b (Alba) based on a similarly positioned proline, although NMR studies of Alba have not been reported to our knowledge. The absence of a similarly positioned proline in Sso10b2 leads to a single protein conformation under conditions suitable for long-term NMR data accumulation and has facilitated the determination of a high quality NMR solution structure.

The centrifugation, DSC, and NMR data presented here demonstrate that Sso10b2 exists predominantly as a dimer in solution below pH 6, with increased tendency for higher order oligomers near the growth temperature at pH 7. Previous crystal structures have indicated that members of the Alba family of proteins are able to interact via at least three different interfaces. The NMR structure demonstrates that below pH 6 dimerization occurs in solution via the interface observed in crystal structures with the largest buried surface area (interface I). The interface is entirely composed of hydrophobic and hydrogen-bonding interactions, with no evidence for salt-bridge or ion pair networks that are often thought to be important in stabilizing oligomeric hyperthermophile proteins (*43*−*45*).

The charge distribution in Sso10b2 is anisotropic, with a significant positive charge density found on the surface defined by the C-termini of β-strands β_1, β_2, and β_3 (Figure 8). This surface contains 12 arginines in the dimer. A large part of these are contributed by the RDRRR sequence in the loop separating the β_3 and β_4 strands. Arginine-rich sequences are common in RNA binding proteins (*42*, *46*). This region has been previously argued to be a likely site for nucleic acid binding (*14*), and the NMR titration data presented here confirm this. Most importantly, the motif is not conserved in the Alba family, which may indicate that these proteins can serve a number of roles. The location of the motif in the turn between the β_3 and β_4 strands coincides with the region of the homologous DNase I which interacts with DNA. The NH of the central arginine (R75) in the motif was one of the most perturbed of all NHs in the DNA and RNA chemical shift perturbation titrations. This arginine is highly conserved in all the Alba-like proteins. It is noteworthy that the length of the "arm" containing this motif is significantly shorter in Sso10b2 than in other Alba proteins, such as Sso10b (Figure 9). In addition, this arm is less extended in the solution structure of Sso10b2 than in the crystal. The NMR relaxation data indicate significant flexibility in the arm which may explain this difference. Flexibility may be important in allowing adjustment of the structure to fit various nucleic acid targets.

Although Sso10b2 is highly charged, it contains a significant number of surface hydrophobic residues. These are present not only on the interface involved in dimerization but also on the surface of the α_1-helix as well as on the face of the β-sheet opposite to that involved in dimerization. The α_1-helix is especially interesting since it contains residues perturbed by both DNA and RNA binding, although it contains no positively charged residues other than H19 which is largely buried in the hydrophobic core. In contrast, the solvent-exposed surface is entirely negatively charged, and these charges are located at the N-terminus adjacent to the putative nucleic acid binding site. The α_1-helix is involved in protein−protein interactions in a number of crystal structures of Alba proteins and has been proposed to be involved in a dimer-dimer interface in Af1 (*15*). The perturbations observed with nucleic acid titrations may not be due to interactions with the α_1-helix but rather perturbations of protein−protein interactions involving $\alpha_1-\alpha_1$ interactions as observed in the crystal structures of Af1 and other Alba proteins (interface II). These may be present in solution or may be created upon nucleic acid binding due to cooperative interactions.

It is interesting to note the locations of conserved residues in the Alba family of proteins (Figure 1). Many of the more conserved residues play a structural role in defining the IF3-like fold; for example, V34 and L36 contribute to the hydrophobic core, and G40 is apparently necessary for the tight turn at the end of β_2. V47 and L63 on the other hand define the dimer interface, and interestingly, these are conserved in the *Arabidopsis* and human proteins. Conserved residues on the surface may play a more functional role, for example, K14, L57, and R75. K14 is especially interesting because it is homologous to the residue acetylated in Sso10b and is conserved even in the human homologue. The exposed hydrophobic residue at position 57 is involved in protein−protein interactions at interface II in some of the crystal structures. It is also adjacent to residues perturbed by nucleic acid binding (Figure 1), and a proline at this position resulted in two conformations in Ssh10b (*41*).

Two-State Structural Transition Preceding Unfolding. The thermal unfolding of Sso10b2 is unusual in that the protein undergoes a two-state structural transition at moderately high temperature that is distinct from dimer (or oligomer) dissociation and unfolding. Dimer dissociation occurs in a second DSC transition at even higher temperature coincident

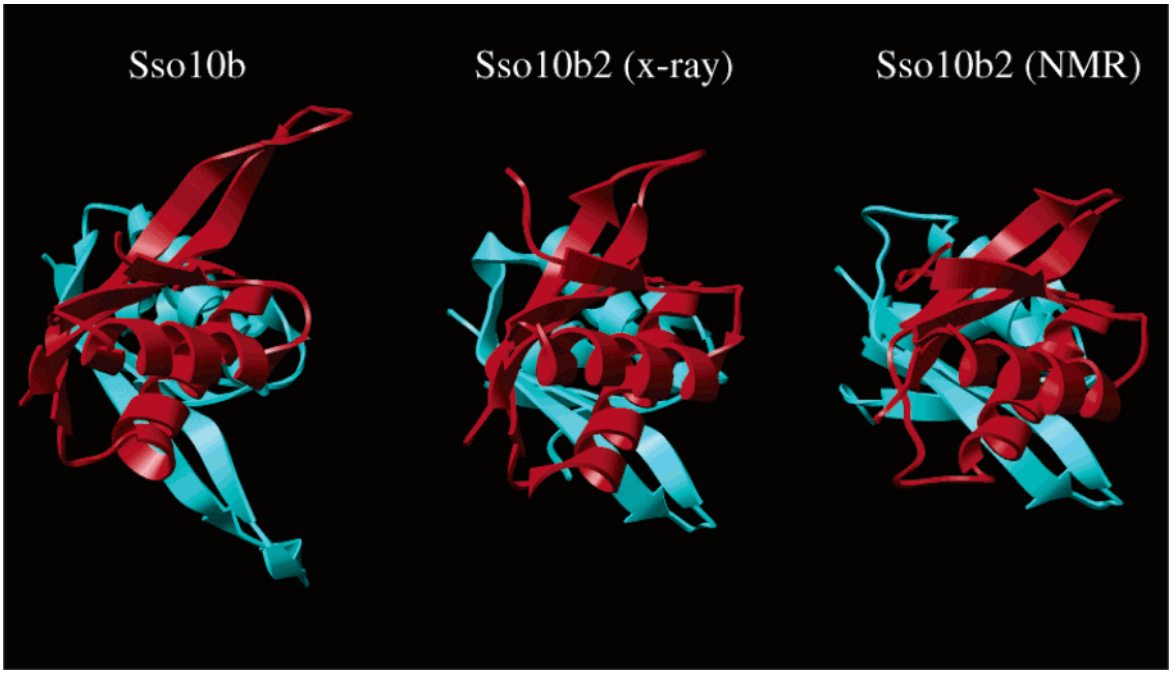

FIGURE 9: Comparison of the NMR solution structure of dimeric Sso10b2 (2A2Y) to the X-ray crystal structures of Sso10b (Alba) (1HOX) and Sso10b2 (1UDV). The monomers in each are distinguished by blue and red shading.

with unfolding. CD spectra indicated that the first transition is associated with conversion of a significant portion of α-helix to *β*-sheet and some increase in random coil. The magnitude of the enthalpy change associated with the transition is large and on the order of that expected for complete unfolding of a protein of comparable size (*47*). Although the cooperativity of the transition increases at pH 7 ($\Delta H_{cal}/\Delta H_{vh}$ ratio < 0.5, indicating increased size of the oligomer participating in the transition), the transition temperature remains independent of concentration and therefore does not represent a change in oligomeric state. While the DSC data may indicate increased oligomerization near neutral pH, this does not necessarily mean that higher order oligomers occur at lower temperature where many physical measurements of molecular size are commonly performed (e.g., gel filtration chromatography, electrophoresis, chemical cross-linking, and analytical ultracentrifugation). The equilibrium constant for tetramer and higher order oligomers may be temperature-dependent such that pronounced oligomerization may be obvious only at higher temperature approaching the growth temperature of *S. solfataricus*. Previous NMR studies of Ssh10b indicated two conformational states, but this was due to cis−trans isomerization of a single proline which is not present in Sso10b2. The possibility remains, however, that the two-state transition observed here is related to that seen in Ssh10b and that the presence of proline in that protein shifts the midpoint of the equilibrium to lower temperature. The extent of the structural change due to proline isomerization in Ssh10b has not been described.

Chemical denaturation of Sso10b2 at pH 7 is consistent with the same three-state model used to explain the DSC results, and the thermodynamic parameters determined by chemical and thermal denaturation agree relatively well with each other. The absence of a change in protein anisotropy in the first transition indicates that this transition is due to a conformational change in the dimer with little alteration of hydrodynamic properties. The second transition, however, exhibits a large change in anisotropy, as expected for protein unfolding to extended chains. Furthermore, the chemical denaturation analysis indicates that the N_2 state becomes significantly populated at high temperatures, and thus, thermal unfolding proceeds through an N_2 intermediate. In contrast, chemically induced unfolding at low temperatures proceeds directly from the N_1 dimer state to unfolded monomers without undergoing the N_1 to N_2 conformational transition.

Comparison of NMR and X-ray Structures of Sso10b2. The NMR solution structure and crystal structure of Sso10b2 are in good agreement with a 2.1 Å rmsd for the Cα atoms. The greatest variation occurs in the N-terminus which is ill-defined by both the NMR and X-ray data. More importantly, the relative alignment of the two monomers differs slightly in the two structures, with the NMR structure slightly more compact than the X-ray structure. The position of C-termini of the α_1-helices in the NMR and X-ray structures differs by about 4 Å. In addition, the two "arms" are splayed outward more in the X-ray structure than in the NMR, so that the Cα carbons of R75 are about 4 Å further away from the center of the dimer in the X-ray structure. The difference most likely results from a flexibility in the arms and adaptation to the packing forces in the crystal.

IF3-like Proteins and Nucleic Acid Binding. Members of the Alba family show significant structural homology to the C-terminal domain of *B. stearothermophilus* IF3, the IF3 subunit of the 30S ribosome of *Thermus thermophilus*, and the N-terminal domain of bovine pancreatic DNase I. Structures of all three have been determined in complex with nucleic acid, and it is reasonable to ask if these can be used to propose a structure for an Sso10b2−nucleic acid complex. Unfortunately, such an approach does not appear promising, since the nucleic acid binding sites in DNase I and the IF3 proteins are significantly different. The *β*-hairpin loop in DNase I plays an important role in binding to the minor

groove of DNA, while in IF3, the primary RNA interaction involves the α_1-helix. Chou et al. (*14*) have argued that K12, K14, and H19 in Sso10b2 are homologous to R89, K102, and F99 in IF3-C. The evidence for this is not exceptionally strong. While H19 (in Sso10b2) and F99 (in IF3-C) are both buried at the interface between α_1 and β_1, K12 and K14 are in the loop between the two segments in Sso10b2, and R89 and K102 are in the middle of α_1 and β_1 in IF3-C and are not similarly positioned. Finally, the symmetry of the Sso10b2 (and Sso10b) dimer has no analogue in the IF3 and DNase I structures. A more productive understanding of nucleic acid binding by members of the Alba family must await determinations of structures of the proteins complexed to RNA and DNA.

REFERENCES

1. Grote, M., Dijk, J., and Reinhardt, R. (1986) Ribosomal and DNA binding proteins of the thermoacidophilic archaebacterium *Sulfolobus acidocaldarius*, *Biochim. Biophys. Acta 873*, 405−413.
2. Guo, R., Xue, H., and Huang, L. (2003) Ssh10b, a conserved thermophilic archaeal protein, binds RNA in vivo, *Mol. Microbiol. 50*, 1605−1615.
3. Marsh, V. L., Peak-Chew, S. Y., and Bell, S. D. (2005) Sir2 and the acetyltransferase, Pat, regulate the archael chromatin protein, Alba, *J. Biol. Chem. 280*, 21122−21128.
4. Bell, S. D., Botting, C. H., Wardleworth, B. N., Jackson, S. P., and White, M. F. (2002) The interaction of Alba, a conserved archaeal chromatin protein, with Sir2 and its regulation by acetylation, *Science 296*, 148−151.
5. Forterre, P., Confalonieri, F., and Knapp, S. (1999) Identification of the gene encoding archeal-specific DNA-binding proteins of the Sac10b family, *Mol. Microbiol. 32*, 669−670.
6. White, M. F., and Bell, S. D. (2002) Holding it together: chromatin in the archaea, *Trends Genet. 18*, 621−626.
7. Aravind, L., Iyer, L. M., and Anantharaman, V. (2003) The two faces of Alba: the evolutionary connection between proteins participating in chromatin structure and RNA metabolism, *Genome-Biology 4*, R64.
8. Lurz, R., Grote, M., Dijk, J., Reinhardt, R., and Dobrinski, B. (1986) Electron microscopic study of DNA complexes with proteins from the archaebacterium *Sulfolobus acidocaldarius*, *EMBO J. 5*, 3715−3721.
9. Reddy, T. R., and Suryanarayana, T. (1989) Archaebacterial histone-like proteins, *J. Biol. Chem. 264*, 17298−17308.
10. Bohrmann, B., Kellenberger, E., Arnold-Schulz-Gahmen, B., Sreenivas, K., Suryanarayana, T., Stroup, D., and Reeve, J. N. (1994) Localization of Histone-like proteins in thermophilic archaea by immunogold electron microscopy, *J. Struct. Biol. 112*, 70−78.
11. Xue, H., Guo, R., Wen, Y., Liu, D., and Huang, L. (2000) An abundant DNA binding protein from the hyperthermophilic archaeon *Sulfolobus shibatae* affects DNA supercoiling in a temperature-dependent fashion, *J. Bacteriol. 182*, 3929−3933.
12. Xu, S., Qin, S., and Pan, X. M. (2004) Thermal and conformational stability of Ssh10b protein from archaeon *Sulfolobus shibattae*, *Biochem. J. 382*, 433−440.
13. Wardleworth, B. N., Russell, R. J., Bell, S. D., Taylor, G. L., and White, M. F. (2002) Structure of Alba: an archaeal chromatin protein modulated by acetylation, *EMBO J. 21*, 4654−4662.
14. Chou, C. C., Lin, T. W., Chen, C. Y., and Wang, A. H. (2003) Crystal structure of the hyperthermophilic archaeal DNA-binding protein Sso10b2 at a resolution of 1.85 angstroms, *J. Bacteriol. 185*, 4066−4073.
15. Zhao, K., Chai, X., and Marmorstein, R. (2003) Structure of a Sir2 substrate, Alba, reveals a mechanism for deacetylation-induced enhancement of DNA binding, *J. Biol. Chem. 278*, 26071−26077.
16. Wang, G., Guo, R., Bartlam, M., Yang, H., Xue, H., Liu, Y., Huang, L., and Rao, Z. (2003) Crystal structure of a DNA binding protein from the hyperthermophilic euryarchaeon *Methanococcus jannaschii*, *Protein Sci. 12*, 2815−2822.
17. Biou, V., Shu, F., and Ramakrishnan, V. (1995) X-ray crystallography shows that translational initiation factor IF3 consists of two compact alpha/beta domains linked by an alpha-helix, *EMBO J. 14*, 4056−4064.
18. Lahm, A., and Suck, D. (1991) DNase I-induced DNA conformation. 2. A structure of a DNase I−octamer complex, *J. Mol. Biol. 222*, 645−667.
19. Gill, S., and von Hippel, P. (1989) Calculation of protein extinction coefficients from amino acid sequence data, *Anal. Biochem. 182*, 319−326.
20. Eisenberg, D., and Crothers, D. (1979) *Physical Chemistry with Applications to the Life Sciences*, Benjamin/Cummings, Menlo Park, CA.
21. Wyman, J., and Gill, S. J. (1990) *Binding and Linkage: Functional Chemistry of Biological Macromolecules*, University Science Books, Mill Valley, CA.
22. Pace, C. N. (1986) Determination and analysis of urea and guanidine hydrochloride denaturation curves, *Methods Enzymol. 131*, 266−280.
23. Sreerama, N., and Woody, R. W. (2000) Estimation of protein secondary structure from CD spectra: comparison of CONTIN, SELCON and CDSSTR methods with an expanded reference set, *Anal. Biochem. 282*, 252−260.
24. Markley, J. L., Bax, A., Arata, Y., Hilbers, C. W., Kaptein, R., Sykes, B. D., Wright, P. E., and Wuthrich, K. (1998) Recommendations for the presentation of NMR structures of proteins and nucleic acids, *J. Mol. Biol. 280*, 933−952.
25. Delaglio, F., Grzesiek, S., Vuister, G. W., Zhu, G., Pfeifer, J., and Bax, A. (1995) NMRPipe: a multidimensional spectral processing system based on UNIX pipes, *J. Biomol. NMR 6*, 277−293.
26. Johnson, B. A. (2004) Using NMRView to visualize and analyze the NMR spectra of macromolecules, *Methods Mol. Biol. 278*, 313−352.
27. Ruckert, M., and Otting, G. (2000) Alignment of biological macromolecules in novel nonionic liquid crystalline media for NMR experiments, *J. Am. Chem. Soc. 122*, 7793−7797.
28. Farrow, N. A., Muhandiram, R., Singer, A. U., Pascal, S. M., Kay, C. M., Gish, G., Shoelson, S. E., Pawson, T., Forman-Kay, J. D., and Kay, L. E. (1994) Backbone dynamics of a free and phosphopeptide-complexed Src homology 2 domain studied by ^{15}N NMR relaxation, *Biochemistry 33*, 5984−6003.
29. Korzhnev, D. M., Skrynnikov, N. R., Millet, O., Torchia, D. A., and Kay, L. E. (2002) An NMR experiment for the accurate measurement of heteronuclear spin-lock relaxation rates, *J. Am. Chem. Soc. 124*, 10743−10753.
30. Mandel, A. M., Akke, M., and Palmer, A. G., III (1995) Backbone dynamics of *Escherichia coli* ribonuclease HI: correlations with structure and function in an active enzyme, *J. Mol. Biol. 246*, 144−163.
31. Tollinger, M., Forman-Kay, J. D., and Kay, L. E. (2002) Measurement of side-chain carboxyl pK_a values of glutamate and aspartate residues in an unfolded protein by multinuclear NMR spectroscopy, *J. Am. Chem. Soc. 124*, 5714−5717.
32. Yamazaki, T., Forman-Kay, J. D., and Kay, L. E. (1993) Two-dimensional NMR experiments for correlating $^{13}C\beta$ and $^{1}H\delta/\epsilon$ chemical shifts of aromatic residues in ^{13}C-labeled proteins via scalar couplings, *J. Am. Chem. Soc. 115*, 11054−11055.
33. Zwahlen, C., Legault, P., Vincent, S. J. F., Greenblatt, J., Konrat, R., and Kay, L. E. (1997) Methods for measurement of intermolecular NOEs by multinuclear NMR spectroscopy: application to a bacteriophage λ N-peptide/*box B* RNA complex, *J. Am. Chem. Soc. 119*, 6711−6721.
34. Linge, J. P., Habeck, M., Rieping, W., and Nilges, M. (2003) ARIA: automated NOE assignment and NMR structure calculation, *Bioinformatics 19*, 315−316.
35. Schwieters, C. D., Kuszewski, J. J., Tjandra, N., and Clore, G. M. (2003) The Xplor-NIH NMR molecular structure determination package, *J. Magn. Reson. 160*, 65−73.
36. McGhee, J., and von Hippel, P. (1974) Theoretical aspects of DNA−protein interactions: co-operative and non-cooperative binding of large ligands to a one-dimensional homogeneous lattice, *J. Mol. Biol. 86*, 469−489.
37. Tugarinov, V., and Kay, L. E. (2003) Quantitative NMR studies of high molecular weight proteins: application to domain orientation and ligand binding in the 723 residue enzyme malate synthase G, *J. Mol. Biol. 327*, 1121−1133.
38. She, Q., Singh, R. K., Confalonieri, F., Zivanovic, Y., Allard, G., Awayez, M. J., Chan-Weiher, C. C., Clausen, I. G., Curtis, B. A., De Moors, A., Erauso, G., Fletcher, C., Gordon, P. M., Heikamp-de Jong, I., Jeffries, A. C., Kozera, C. J., Medina, N.,

Peng, X., Thi-Ngoc, H. P., Redder, P., Schenk, M. E., Theriault, C., Tolstrup, N., Charlebois, R. L., Doolittle, W. F., Duguet, M., Gaasterland, T., Garrett, R. A., Ragan, M. A., Sensen, C. W., and Van der Oost, J. (2001) The complete genome of the crenarchaeon *Sulfolobus solfataricus* P2, *Proc. Natl. Acad. Sci. U.S.A. 98*, 7835−7840.

39. van Holde, K. E., and Weischet, W. O. (1978) Boundary analysis of sedimentation velocity experiments with monodisperse and paucidisperse solutes, *Biopolymers 17*, 1387−1403.
40. Lubben, M., and Schafer, G. (1989) Chemiosmotic energy conversion of the archaebacterial thermoacidophile *Sulfolobus acidocaldarius*: oxidative phosphorylation and the presence of an F0-related N,N′-dicyclohexylcarbodiimide-binding proteolipid, *J. Bacteriol. 171*, 6106−6116.
41. Cui, Q., Tong, Y., Xue, H., Huang, L., Feng, Y., and Wang, J. (2003) Two conformations of archaeal Ssh10b. The origin of its temperature-dependent interaction with DNA, *J. Biol. Chem. 278*, 51015−51022.
42. Weiss, M. A., and Narayana, N. (1998) RNA recognition by arginine-rich peptide motifs, *Biopolymers 48*, 167−180.
43. Karshikoff, A., and Ladenstein, R. (2001) Ion pairs and the thermotolerance of proteins from hyperthermophiles: a "traffic rule" for hot roads, *Trends Biochem. Sci. 26*, 550−556.
44. Kumar, S., and Nussinov, R. (2001) How do thermophilic proteins deal with heat?, *Cell. Mol. Life Sci. 58*, 1216−1233.
45. Kumar, S., and Nussinov, R. (2004) Different roles of electrostatics in heat and in cold: adaptation by citrate synthase, *ChemBioChem 5*, 280−290.
46. Jones, S., Daley, D. T., Luscombe, N. M., Berman, H. M., and Thornton, J. M. (2001) Protein−RNA interactions: a structural analysis, *Nucleic Acids Res. 29*, 943−954.
47. Robertson, A. D., and Murphy, K. P. (1997) Protein structure and the energetics of protein stability, *Chem. Rev. 97*, 1251−1267.

BI051266R